Photonic generation and detection of W-band OCDMA signals

Morad Khossravi Eghbal,[a,*] Mehdi Shadaram,[a]
[a]University of Texas at San Antonio, Electrical and Computer Engineering Department, One UTSA Circle, San Antonio TX, USA, 78249

Abstract. We have designed and studied a W-band OCDMA radio-over-fiber system. To increase the number of channels, optical encoding and decoding are utilized. The theoretical analysis of generation, modulation and optical encoding of a signal is presented. Also, to confirm the theoretical analysis, the transmission of the encoded signal, decoding and its detection is simulated. Two optical codes (m-sequence and quaternary phase shift) with different code lengths are used and the results are presented. Simulation results for each set of codes are compared and the performance of each code is evaluated in the final bit error rate measurements. The quaternary phase shift codes show almost 20 dB of BER gain compared to m-sequence. In addition, the number of channels that are accommodated by the quaternary phase shift codes are more than four times the m-sequence code with the same length. The stability of the system is improved by using a low-frequency sinewave generator to modulate the signal to the W-band. Also, the capacity and reach of the system are improved while the cost and complexity are reduced by eliminating the necessity of using a high-frequency sinewave generator in the modulator. This system simultaneously guarantees increased capacity and reach for a radio-over-fiber network.

Keywords: radio-over-fiber, millimeter waves, optical code division multiplexing, dual-electrode Mach Zehnder modulator

***** Correspondence Author**,** E-mail: morad.khosravieghbal@utsa.edu

1 Introduction

The introduction of data services and applications that require higher bandwidth and augmented bitrates is dramatically increasing[1,2,19-21]. Services such as live broadcasting and video streaming demand a larger bandwidth along with minimal latency and enhanced reliability[3]. Thus, the mainstream of the future mobile communication is governed by how much bandwidth can be dedicated to such services and therefore how the capacity of the network can be improved to keep up with the growing demand for bandwidth. An effective method to increase the capacity of a network is to migrate to higher frequency bands. The millimeter wave region has promising features that can accommodate large capacity at frequencies in the V- and W-band region[4,19-21]. Also, it offers enhanced security based on its narrow beam width antenna and higher attenuation in the free space propagation, making it only available across its designated coverage area[5-7].

The latter can be overcome by the introduction of radio-over-fiber (RoF) techniques in which a millimeter wave signal (radio frequency wave) can be transmitted through the optical fiber to effectively increase the propagation distance compared to the free space propagation[8].

Radio-over-fiber guarantees mobility with an acceptable level of quality of service (QoS) in combination with other methods such as free space optics (FSO) or visible light communication. Moreover, since RoF can transmit a large capacity of data (multi-Gb/s) through optical fiber, it has an outstanding advantage over lower frequency bands.[23-25]

There are several millimeter wave generation methods that have been suggested in the literature[9-12,27-29,38]. Yang et al. investigated a myriad of methods to generate millimeter waves including the OSSB modulation through a dual-electrode Mach Zehnder modulator (DE-MZM). Also, Yang et al. explained that this method is based on WDM demultiplexing where two coherent optical carriers are used to generate radio frequency to be transmitted through the fiber[24]. Bekkali and Nishimura[25] suggest a coherent RoF system to transmit high-capacity millimeter wave links as a backup fiber network to increase the resilience as well as transmission distance. The most common method of millimeter wave generation is by passing the baseband laser signal through a Mach Zehnder modulator (MZM) that is driven by the signal generator working at the desired millimeter wave frequency[12,14,25,28-29]. In this method, the baseband signal is directly up-converted to the higher millimeter wave bands. However, this method requires high-frequency (in the millimeter wave region) signal generators that are stable and precise.

The utilised method of signal generation for this work is based on tandem DE-MZM that are driven by signal generators operating at frequencies below 30 GHz[14]. The reason that a tandem DE-MZM is used is to increase the spectral efficiency and to use both side bands to transmit two individual signals per side band. Plus, the scheme used to create multiple harmonics will enable

the designer to dynamically switch the select carriers and to change the millimeter wave signal without needing to change the oscillators. This method of generation increases the spectral efficiency, flexibility, and the stability of the system. To generate the millimeter wave signal at the desired frequency, two signal components with the frequency difference equal to the millimeter wave frequency of choice are selected and transmitted through the fiber to the receiver. On the receiver's side, they are heterodyned at a photodiode to generate the desired millimeter wave signal.

Also, the optical code division multiple access (OCDMA) can assist in increasing system capacity by applying optical coding to the signals. The application of OCDMA introduces a specific orthogonal optical code for each channel. With this technique, a single wavelength can be shared between more than one channel (depending on the length of the code) and thus increase the capacity of the system multifold[12-14]. Also, it contributes to the security of the transmission as only the matching codes can decode the encoded signals. Therefore, only authorized channels can have access to their individual signals and thus, the decoded signals for an unauthorized channel would be noise.

Erdogan gave a comprehensive analysis of the superstructure fiber Bragg grating (SSFBG) and its significance in encoded and decoding signals optically for OCDMA systems[26]. In addition, Dai et al compared the performance of 0/π-phase-shift SSFBG and ± π/2-phase-shifted SSFBG in terms of the security, coding and system preferences. Researchers discussed different codeword assignments to SSFBGs[34] while other papers discuss various other properties of encoding with SSFBGs such as different codes[32,33,35], error probability[36-37] and the quality of encoded signals' profile for different settings[39-40].

In this paper, we have analyzed optical signal generation, modulation and optical encoding and then we studied the results obtained from software simulation of the signal's transmission through a 50-km length of optical fiber and observed the effectiveness of optical encoding/decoding in increasing the number of channels. In addition, we have investigated the effects of two different sets of optical codes that are encoded in a SSFBG device to increase the number of channels to six[13,22]. The contribution of this work is the analysis and simulation of such optically encoded radio-over-fiber systems that operate at W-band frequencies (84 GHz) with optical codes chosen from m-sequence and quaternary phase shift code families. The novelty of the paper is in the incorporation of optical encoding (using both m-sequence and quaternary phase shift codes) with W-band radio-over-fiber communication. There is no previous work that has used OCDMA techniques for W-band signals that utilize quaternary phase shift codes and m-sequence codes as the optical encoding formats

2 Theoretical Analysis

Fig. 1 illustrates a detailed schematic of the system that is analyzed for an optical signal. The optical signal generated by a Continuous Wave laser has the mathematical expression of the form:

$$\mathrm{E}_{out_{laser}} = \mathrm{E}_{in}.\, e^{-j\omega_c t} \tag{1}$$

Then this $\mathrm{E}_{out_{laser}}$ is fed to the input of the first DE-MZM. The upper arm is biased by a dc voltage source of $\frac{V\pi}{2}$ and the lower arm is connected to the ground. The dc voltage difference

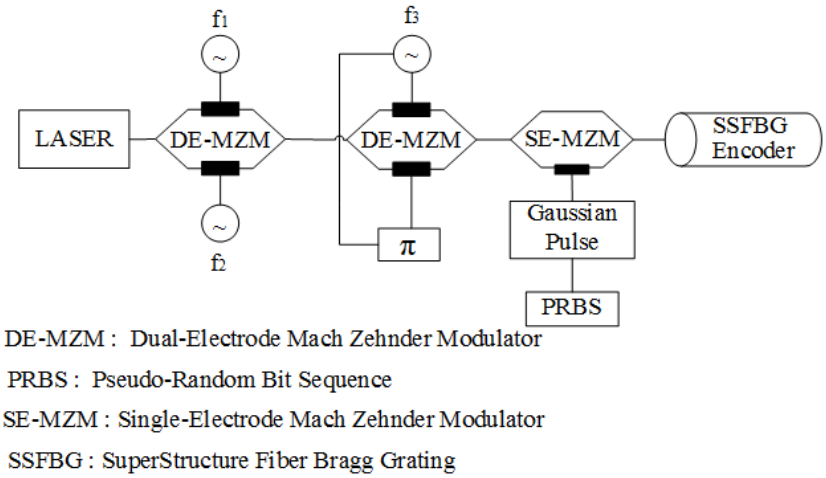

Fig. 1 Theoretical analysis block diagram. This figure shows the basic devices needed to upconvert the baseband signal from the laser to radio frequencies (millimeter wave region)

between the two arms is set at $\frac{V\pi}{2}$ which means that the first DE-MZM is biased at the quadrature point. The output of the first DE-MZM will be:

$$E_{DEMZM_1} = \frac{E_{in}}{2} . \cos(\omega_c t) . \{\cos\ (a_2\pi . \cos(\omega_{rf2}t) + a_1\pi . \cos\left(\omega_{rf1}t + \frac{\pi}{2}\right) + \frac{\pi}{2}) + \cos\ (a_1\pi . \cos(\omega_{rf1}t) + a_2\pi . \cos\left(\omega_{rf2}t + \frac{\pi}{2}\right)\} \quad (2)$$

Where a1 = $\frac{V_{ac1}}{V_\pi}$, a2 = $\frac{V_{ac2}}{V_\pi}$, ωrf1 = 2πf1 and ω_{rf2} = 2πf2. By introducing Jacobi-Anger expansion derivations from the Bessel functions $J_n(x)$, we can rewrite (2) to a more intuitive format:

$$E_{DEMZM_1} = \frac{E_{in}}{2} . \cos(\omega_c t) . \{-2\ J_1(a_2\pi) .\ J_0(a_1\pi) . \cos\ (\omega_{rf2}t) - 2\ J_1(a_2\pi) . J_2(a_1\pi) . \cos\ (\omega_{rf2}t + 2\omega_{rf1}t) -\ 2\ J_1(a_2\pi) . J_2(a_1\pi) . \cos\ (\omega_{rf2}t - 2\omega_{rf1}t)\} \quad (3)$$

The output of the first DE-MZM is then launched into the second DE-MZM. The upper arm is biased by a dc voltage current equal to + $\frac{V\pi}{2}$ and an ac sinusoidal signal source

cos ($\omega_{rf3}t$) where $\omega_{rf3} = 2\pi f$. The lower arm is biased by another dc voltage source of $-\frac{V\pi}{2}$ and a π-phase shifted replica of the upper arm's signal source. The dc voltage difference between the two arms is Vπ, which means the second DE-MZM is biased at the null point.

The output of the second DE-MZM will be:

$$E_{DEMZM_2} = E_{DEMZM_1}.\{\cos(a_3\pi.\cos(\omega_{rf3}t) + \frac{\pi}{2}) + \cos(a_3\pi.\cos(\omega_{rf3}t - \frac{\pi}{2}))\} =$$

$$E_{DEMZM_1}.\{-\sin(a_3\pi.\cos(\omega_{rf3}t)) + \cos(a_3\pi.\sin(\omega_{rf3}t))\} \quad (4)$$

By rewriting (4) using the Jacobi-Anger expansion derivations from the Bessel functions, we will have:

$$E_{DEMZM_2} = E_{DEMZM_1}.\{-4\,J_1(a_3\pi).\cos(\omega_{rf3}t)\} \quad (5)$$

Now if we expand (5) by using the Bessel functions and filtering out the terms that do not contribute to the two carriers at 1552.97 nm and 1553.65 nm the output is:

$$E_{DEMZM_2} = 4J_0(a_1\pi).J_1(a_2\pi).J_1(a_3\pi).\cos(\omega_{rf2}t + \omega_{rf3}t)$$
$$+ 4J_0(a_1\pi).J_1(a_2\pi).J_1(a_3\pi).\cos(\omega_{rf2}t - \omega_{rf3}t) - 4J_0(a_2\pi).J_1(a_1\pi).J_1 -$$
$$4J_0(a_2\pi).J_1(a_1\pi).J_1(a_3\pi).\sin(\omega_{rf1}t - \omega_{rf3}t) \quad (6)$$

Where, $(\omega_{rf2}t \pm \omega_{rf3}t)$ relates to the uncoded component's frequency and $(\omega_{rf1}t \pm \omega_{rf3}t)$ are the frequency components of the data modulated signal. The modulated portion of (6) becomes:

$$E_{DEMZM_{2mod}} = -4J_0(a_2\pi).J_1(a_1\pi).J_1 - 4J_0(a_2\pi).J_1(a_1\pi).J_1(a_3\pi).\sin(\omega_{rf1}t - \omega_{rf3}t) \quad (7)$$

Therefore, the data modulated component is directed to the single-electrode MZM (SE-MZM) for data modulation. The pseudo-random data sequence (d(t) ≡ {1,0}) is shaped by a Gaussian pulse shaper (GPS) that convolutes each '1' bit of the PRBS stream into Gaussian pulses with

full width half maximum (FWHM) of 5.2 ps, generating a shaped bit stream of '1's and '0's named DG(t). The output of the SE-MZM is:

$$E_{SEMZM} = E_{DEMZM_{2_{mod}}} . \sin\left(\frac{\pi . DG(t)}{V_{\pi}}\right) \quad (8)$$

After being data-modulated, the signal is passed to the SSFBG device to be optically encoded. The impulse response of the SSFBG (for the encoder configuration, h_p^{en}) is shown below[15-16]:

$$h_p^{en} = h_{chip}(t) * \sum_{k=1}^{N} a_{p,k}^{en} \exp\left(j\varphi_{p,k}^{en}\right) \delta(t - kt_{ch}) \quad (9)$$

Where, $h_{chip}(t)$ is each segment of the code's impulse response, $a_{p,k}^{en}$ and $\varphi_{p,k}^{en}$ are amplitude and phase components defined by the code and finally $\delta(t - kt_{ch})$ is the pulse train separated by the length of each segment t_{ch}. The encoding happens in the variations of phase between two consecutive segments of the code ($\exp\left(j\varphi_{p,k}^{en}\right)$) . Depending on the level of variation (two level: 0 and π or four level: 0, π/2, π and 3π/2), the phase shifts are translated into different optical profiles of the encoded modulated optical signal. To decode the signal, these variations are identically kept but simply inversed to convert the encoded optical profile into the original profile before encoding.

The bit error rate of an OCDMA system employing SSFBGs for encoding/decoding where the signal is time-spread after encoding is given by the following equation[30-32].

$$P_e \cong 1 - \varphi\left[\left(\frac{N_0}{2E_b} + \frac{1}{6N^3} \sum_{k=1,\ k\neq i}^{K} r_{k,i}\right)^{-\frac{1}{2}}\right] \quad (10)$$

Where E_b is the bit energy, $N_0/2$ is the two-sided spectral density of an additive white Gaussian noise (AWGN) channel noise process, φ is the normalized (zero mean unit variance) Gaussian cumulative distribution function, K is the number of simultaneous users, and $r_{k,i}$ is a function of the aperiodic autocorrelation functions C_k, $_k(l) = C_k$ (l) and C_i, $_i(l) = C_i(l)$ of the codes k and i [33] defined as:

$$r_{k,i} = 2N^2 + 4\sum_{l=1}^{N-1} C_k(l)C_i(l) + \sum_{l=1-N}^{N-1} C_k(l)C_i(l+1) \quad (11)$$

2.1 Optical Encoding

To investigate the effect of coding schemes on the output of the system as well as different system characteristics, we introduced another method of encoding to the optical pulse to fulfil the requirements of OCDMA signal expansion. Also, optical encoding will help to increase the capacity of the system by accommodating more channels. But there is a trade-off between the length of the code (latency of the system) and the number of channels that are added to the system. The ideal case is a relatively short code (less number that generates a larger number of codes with enhanced cross-correlation characteristics that can be assigned to different channels. In addition, when an encoded signal is decoded with a code profile other than its designated encoded profile, the output would contain a noise-like series of peaks and dips with no significant high-amplitude peak to represent a digital '1'. Thus, with this scheme, all the digital '1's in the data set generated from the PRBS and shaped by the Gaussian wave generator will be detected if the signal is passed through the correct decoder. Otherwise '1' will be detected as '0'.

The optical encoding in a SSFBG device accommodates the optical signal's seamless transmission across the network without needing any electrical/optical or optical/electrical conversion. Any conversion between optical and electrical domain and vice versa would attenuate the signal power significantly as well as imposing a lot of noise in the O/E and E/O conversion process. Also, another advantage of encoding/decoding in SSFBG would be is its very small footprint compared to electronic encoders. Finally, the phase shift between two consecutive segments can be controlled more accurately than electronic encoders since SSFBGs introduce a relatively precise phase shift based on the refractive index change and their length. However, the disadvantage of SSFBGs are high cost of manufacturing and lack of flexibility.

Once a code is etched on the device, it will be permanently there, so it can only be used for a certain code.

The codes used to encode the signal optically shall be etched to a SSFBG with appropriate length and features with an UV light with right power and frequency to prepare the SSFBG for encoding purposes. Thus, once etched, it can no longer be changed and used for another code. If another code should be used, that code has to be etched on a new SSFBG which a time consuming and costly process is. Therefore, this system is ideal for users that will use a certain code for a longer length of time before switching the hardware.

2.1.1 M-sequence codes

The m-sequence codes are well defined and used in the literature[12-14]. The type of codes that have been used in this research are unipolar codes (the phase shifts are two levels: 0 and π) with 31 segments. Table 1 shows the number of shift registers and the corresponding code segments for a m-sequence code. Per Table 1, a 31-segment code can generate up to six codes that can accommodate six individual channels. These codes are listed in Table 2.

Table 1 M-sequence code lengths and the number of Linear Feedback Shift Register sequences (adopted from [17])

# of shift registers (n)	**# of code segments ($N = 2^n-1$)**	**# of codes generated ($N_p(n)$)**
2	3	1
3	7	2
4	15	2
5	31	6
6	63	6
7	127	18
8	255	16
9	511	48
10	1023	60

Table 2 Unipolar M-sequence codes for six channels

Encoder#	**M-sequence code**
Encoder 1	00ππ0πππ0π0π0000π00π0ππ00πππππ0
Encoder 2	0π00ππ0000π0ππ0π0π0π000πππ0πππππ0
Encoder 3	ππ00πππ0000ππ0π0π00π000π0πππππ0
Encoder 4	πππ000π0π0ππ0π0000ππ00π00πππππ0

Encoder 5	π000π00π0π0ππ0000πππ00ππ0πππππ0
Encoder 6	0ππ0π00π0000π0π0πππ0πππ00πππππ0

2.1.2 Quaternary phase shift codes

The studied alternative coding scheme here is called quaternary codes[18,22]. These codes are like m-sequence codes except there are four phase levels associated with each code instead of two (0 or π). In this code, each segment can have a value from 0 up to 3 that each represent phase shifts equal to 0, π/2, π and 3π/2 respectively. Like m-sequence codes, this family of codes is generated in a series of shift registers with an initial value. Depending on the initial value (that can take four states), the resulting code would be different. Also, the position of feedback tabs (a_3, a_2, and a_1) can be determined by the following equation where '0' is defined by $c_i = 4$. In this equation, n and i are equal to the number of shift registers and phase levels respectively[18,22]

$$a_i = (c_i - c_1)\, a_{i-1} + (c_i - c_2)\, a_{i-2} + \ldots + (c_i - c_n)\, a_{i-n} \quad (12)$$

For the case of this research, a 3-level shift register was chosen to generate codes with 7 segments (bits).

Therefore, there are two characteristic polynomials (1213 and 1323) generating the characteristic polynomial equation of $f_1(d) = 1d^3 + 2d^2 + 1d + 3$ for 1213 and $f_2(d) = 1d^3 + 3d^2 + 2d + 3$ for 1323. Now, for these two polynomial equations, positions of the feedback tabs are $a_4 = 2a_3 + 3a_2 + a_1$ and $a_4 = a_3 + 2a_2 + a_1$ respectively. For a system with r = 3 shift registers, code length would be $N = 2^r - 1 = 7$ and thus the number of generated orthogonal codes will be $M = 2^r + 1 = 9$. Nine codes are more than four times the number of codes generated by the same length code of the m-sequence (2 codes for code length of 7-segments)[18]. Also, since the code uses 4-level phase changes, the generated codes are more complex making it more difficult to be cracked. Table 3 summarises all nine codes that can be generated from a 3-level shift register

quaternary phase shift code with the characteristic polynomial equation of $f_1(d) = 1d^3 + 2d^2 + 1d + 3$.

For the system that is presented in this research, only six codes (per six channels) are needed. The criteria for selecting the six best codes out of nine generated codes are based on the performance of the codes in the system. The selected ones show a better bit error rate (BER) versus received optical power according to Fig. 7. Therefore, the selected codes for this study are numbers 2, 4, 6, 8, and 9.

2.2 Comparison between M-sequence and Quaternary Phase Shift codes

First, we must realise that the length of the two families of codes is different. The length of the codes used in a system has a direct effect on the bit rate of the system to be able to perfectly decode and retrieve the codes. Thus, the longer the codes, the smaller the bit rate of the system will be. On the other hand, the length of the code also determines the number of the channels than can be accommodated in a system. Therefore, there should be a trade-off between these two important parameters in the system[13,22].

In the first family of codes (m-sequence codes), to be able to accommodate six channels, we had to design the number of segments according to Table 3. Table 3 suggests that to be able to accommodate six channels, and using m-sequence codes, we must have a 31-segment code[17]. A 10 Gb/s system will provide 0.1 ns space for the encoded signal bit to expand (per DS-CDMA characteristics) and yet there will be no interference with the neighboring bit. However, for a

Table 3 Nine 7-segment quaternary phase shift codes generated from $f_1(d)$, the code sequences and their corresponding phase shifts between each segment

Code #	Generated sequence	Quaternary code
1	2002022	π -0-0-π-0-π-π
2	3221211	3π/2-π-π-π/2-π-π/2-π/2
3	1223233	π/2-π-π-3π/2-π-3π/2-3π/2
4	1013102	π/2-0-π/2-3π/2-π/2-0-π

5	1100123	π/2-π/2-0-0-π/2-π-3π/2
6	2010333	π-0-π/2-0-3π/2-3π/2-3π/2
7	1112030	π/2-π/2-π/2-π-0-3π/2-0
8	2133003	π-π/2-3π/2-3π/2-0-0-3π/2
9	2303130	π -3π/2-0-3π/2-π/2-3π/2-0

31-segment code, the expansion would require ~ 0.2 ns, which would cause a severe interference making it very difficult to correctly decode.

Therefore, to maintain the pulse integrity after a 31-segment code expansion, we must either decrease the length of the Gaussian pulse or decrease the bit rate to 4 Gb/s (which will give a 0.25 ns space for expansion). In this research, to be able to decode such codes, by fixing the PRBS Gaussian pulse to a FWHM of 5.2 ps, the bit rate is set to be 4 Gb/s.

The advantage of this code is that the phase of the sequence is only changing between two levels (0 or π) and the generated codes have a good auto- and cross- correlation. This results in the decoded signals having a very distinct peak with negligible side-lobes. On the other hand, because of the increased number of segments, the SSFBG devices are bulkier and these codes introduce larger delays.

The other family of codes (quaternary phase shift codes) can accommodate more channels with shorter lengths from the SSFBG encoder / decoder. A 7-segment code can accommodate nine channels with codes while a 7-segment m-sequence code can only generate two orthogonal codes (see Table 2). Also, they have good auto- and cross-correlation and can easily operate at bit rates as high as 10 Gb/s (since their expansion is limited to only approximately 10 × 5.2 ps which is well within the range of 0.1 ns).

Also, quaternary phase shift codes introduce shorter delays compared to 31-segment m-sequence codes. However, they are more complex than m-sequence codes because they have four phase shift levels instead of two.

2.2.1 Orthogonality of each set of codes

The selected codes (6 × 31-segment m-sequence and 6 × 7-segment quaternary phase shift codes) are selected from the entire range of codes that are possible with the specific segments mentioned. It means that out of all the possibilities to sequence codes in quaternary phase shift codes, the selected 9 codes show the best orthogonal with one another compared to the rest of other possible codes in Family A with the mentioned characteristic polynomial equation. Table 4 gives the orthogonality distance between each m-sequence code. By assuming π's as '1' and 0's as '0' in each sequence, the orthogonality of each sequence against other five sequences is calculated by a bitwise XOR multiplication and then XOR adding each bit by bit. In the final result, if there is an even number of differences between two sequences, the difference between two sequences is 0 and if odd, the difference is 1.

Table 4 Orthogonality of each sequence of 6 m-sequence codes used in this research

Code #	1	2	3	4	5	6
1	0	1	0	1	0	1
2	1	0	0	0	0	1
3	0	0	0	0	1	1
4	1	0	0	0	1	1
5	0	0	1	1	0	1
6	1	1	1	1	1	0

3 Principle of Operation

As is illustrated in Fig. 2, a Continuous Wave laser generates a baseband optical signal at 1553.32 nm with 7 MHz of linewidth and 5 dBm of input power. This signal is launched to the

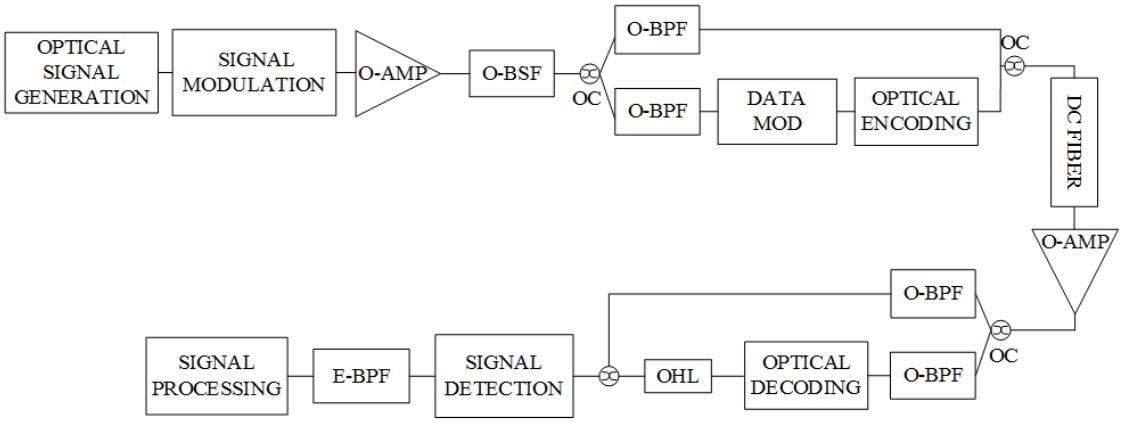

Fig. 2 Simulation setup

first DE-MZM operating in the linear region and driven by two sine wave generators with frequencies set at f_1 = 21 GHz and f_2 = 25 GHz

This signal is launched to the first DE-MZM operating in the linear region and driven by two sine wave generators with frequencies set at f_1 = 21 GHz and f_2 = 25 GHz. Thus, the output spectrum of the first DE-MZM has components at ±21 GHz, ±25 GHz, and ±21±25 GHz. The output spectrum of the first DE-MZM is then input to the second DE-MZM that is driven by an f_3 = 19 GHz sine wave generator and its π shifted copy for each electrode. The output spectrum of the second DE-MZM has components at ±19 GHz and ±19 GHz shifted versions of the input frequency spectrum. An optical amplifier with 30 dB amplification compensates for the attenuation of the two stages of DE-MZM and optical couplers. Also, to avoid the effect of unused high-power components on our carriers, a band-stop filter is used to remove those tones that are not needed.

Out of the output spectrum of the second DE-MZM, two optical carriers, one at 1553.65 nm and the other at 1552.97 nm are selected. The bandwidth of two band pass filters selecting each carrier is 150 MHz. The difference between these two carriers is 0.680 nm which is equal to 84.549 GHz. The carrier at 1553.65 nm is then transmitted to six single-electrode MZM (SE-

MZM) to be data modulated with a 10 Gb/s pseudo-random bit sequence (PRBS) generator with a 2^{31}-1 sequence length that is shaped with a Gaussian wave generator. After data modulation, each of the six data modulated signals is encoded in a SSFBG device to generate individual encoded replicas of the signal based on the optical profile of the SSFBG encoders per each channel.

Consequently, all six encoded signals and the uncoded carrier at 1552.97 nm are aggregated and transmitted through a 50-km length of dispersion compensated fiber to the receiver. Another optical amplifier with 30 dB of amplification compensates for the loss in the fiber and other insertion losses.

On the receiver's side, again the uncoded component and six encoded signals are separated. The six encoded signals are directed to six other SSFBG devices that have a similar but inversed profile relative to the encoders to decode the signals that are encoded in the corresponding encoders' profile. This way, only signals that have similar profiles are successfully decoded. For different profiles, these signals are decoded to noise.

The decoded profile has a distinct peak at '1's and insignificant amplitude at '0's (see Fig. 4 and 6). Therefore, the input bit sequence can be easily regenerated by the help of an optical hard limiter (OHL) having a correct threshold value.

Finally, at the end stage of detection, each decoded signal and uncoded component are heterodyned in an individual photodiode to generate the data modulated millimeter wave signal up-converted to 84 GHz. An electrical bandpass filter then separates the peak at 84 GHz and passes the signal to the detection and signal processing modules. In the case of retransmission through a millimeter wave antenna, the wireless propagation simulation of the detected signal after being filtered is not studied in this work mainly because of unavailability of the required

wireless simulation models in the utilised software (VPI TransmissionMaker) and that the focus of the study is on radio-over-fiber propagation.

3.1 Link budget

The link budget for the entire system is:

(2 × DE-MZMs) + (2 × 1:2 optical couplers) + (~ 10 dB SSFBG loss) + (2 × 1:6 optical couplers) + (0.2 dB/ km × 50 km fiber attenuation)

3.2. Transmission impairments

The impairments that occur in the system affecting the received signal are rooted from and identified in three major sections of the system, the transmitter, the fiber, and the receiver. The major impairments in the transmitter side are the RIN of the laser, the modulation index of the DE-MZMs and SE-MZM, ASE noise of the amplifier, and the nonlinearity of the SSFBG device.

The fiber impairment is nonlinearities and the ASE noise of pre-amplification. However, the input power level to the fiber is designed to be below the threshold to avoid fiber nonlinearites to be invoked.

The major impairments at the receiver are the shot noise and the thermal noise of the photodiode plus the nonlinearity from the SSFBG in decoding the optical signal. The system's parameters are chosen so that these impairments are either compensated or are negligible so the signal propagation is not compromised by them are either compensated or are negligible so the signal propagation is not compromised by them.

4 Simulation Results

The simulation setup for this work was created in VPITransmissionMaker software version 9.7 from VPIPhotonics. Fig. 2 illustrates the setup. The simulation results for each set of codes are presented in the next two sections.

4.1 M-sequence codes

The optical signal generated by the laser enters the first DE-MZM. According to the ac and dc voltage sources driving upper and lower arms of both modulators, the output spectrums of them have several components at different frequencies relative to the centre wavelength of the laser light. Fig. 3 demonstrates the output spectrum of the first and second DE-MZM. The output spectrum of first DE-MZM is directed to the second DE-MZM. Two frequency components that are marked are filtered with two bandpass filters (with a bandwidth of 150 MHz) to serve as the carriers that generate a millimeter wave signal at the photodiode.

Fig. 4 shows the optical profile of four encoded and decoded signals (codes # 1 and # 3 of m-sequence codes). The reason all six codes are not shown is that the trend of encoding and decoding can be understood from the two and also to save space for the results of the other code family. However, all six codes show the same effect in their encoded/decoded profiles. The

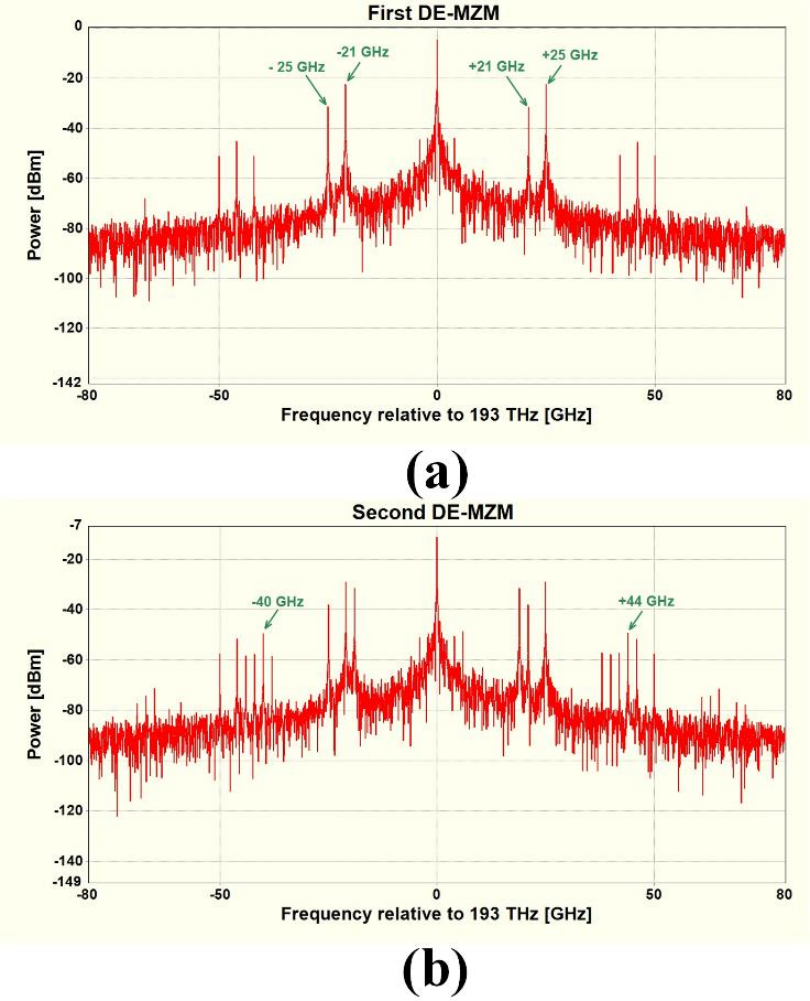

Fig. 3 Output spectrum after DE-MZMs. (a) after the first DE-MZM, (b) after the second DE-MZM

decoded spectrum clearly reconstructs the initially generated data sequence from the PRBS module. Also, Table 1 provides the complete 31-bit sequence of all six m-sequence codes that are used in this work. The BER versus the received optical power for all six channels are shown in Fig. 5 for different received power levels.

4.2 Quaternary Phase Shift codes

To evaluate the performance of the quaternary phase shift codes in the proposed system, the setup in Fig. 2 is used again. Also, the bit rate is fixed at 10 Gb/s. Again, the simulation results

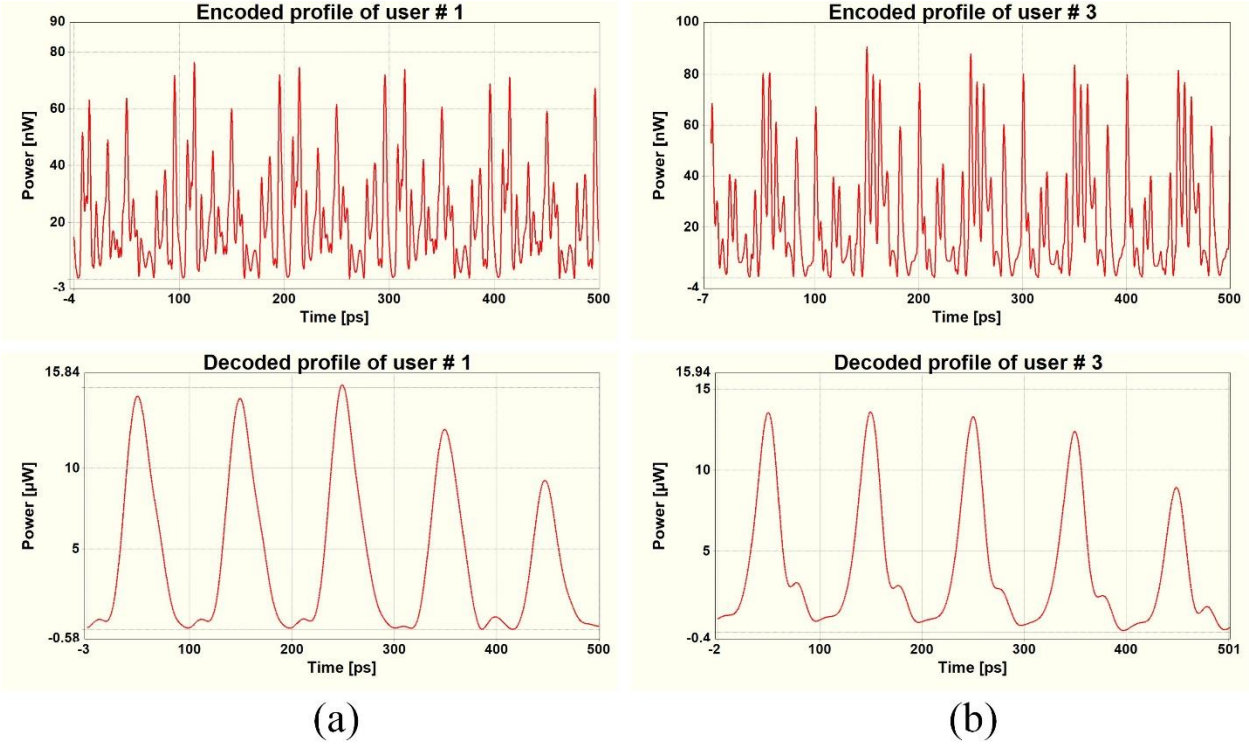

Fig. 4 M-sequence code profiles. (a) encoded profiles of users 1 and 3 (b) decoded profiles of users 1 and 3

are only shown for four codes (code # 2 and # 6 for quaternary phase shift codes). However, the other five codes also show the same result. The encoded and decoded profiles, the BER versus the received optical power diagram, and finally the signal after detection in the photodiode and band pass filtering are illustrated in the following figures. Fig. 6 shows the encoded and decoded profiles of the data-modulated optical signals after passing through the SSFBG device that is encoded and decoded with the three codes from Table 3. Finally, Fig. 7 illustrates the BER value versus the received power in dBm for all nine codes. Based on the performance of the codes, six codes are chosen to accommodate six channels in the system.

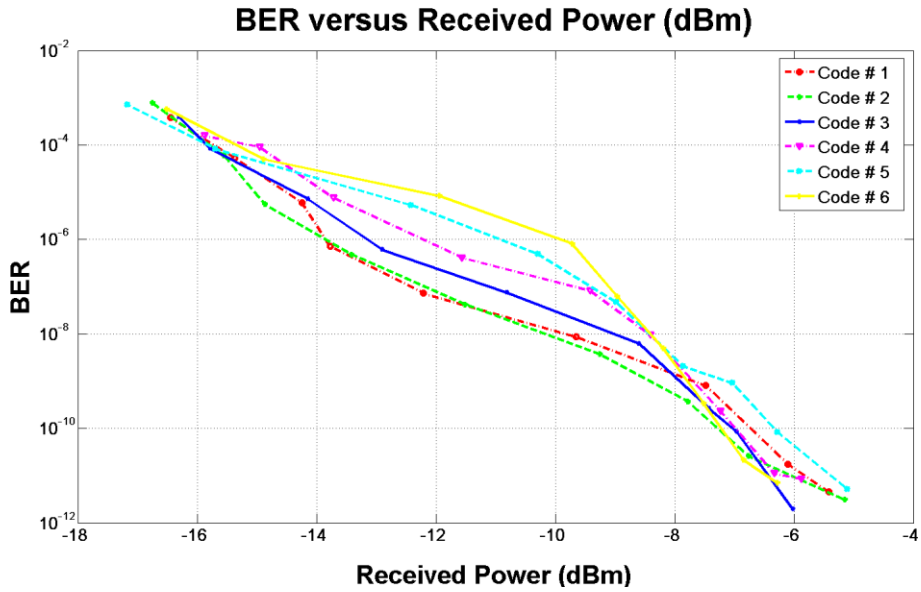

Fig. 5 BER vs. Received Optical power (dBm) for all six M-sequence codes

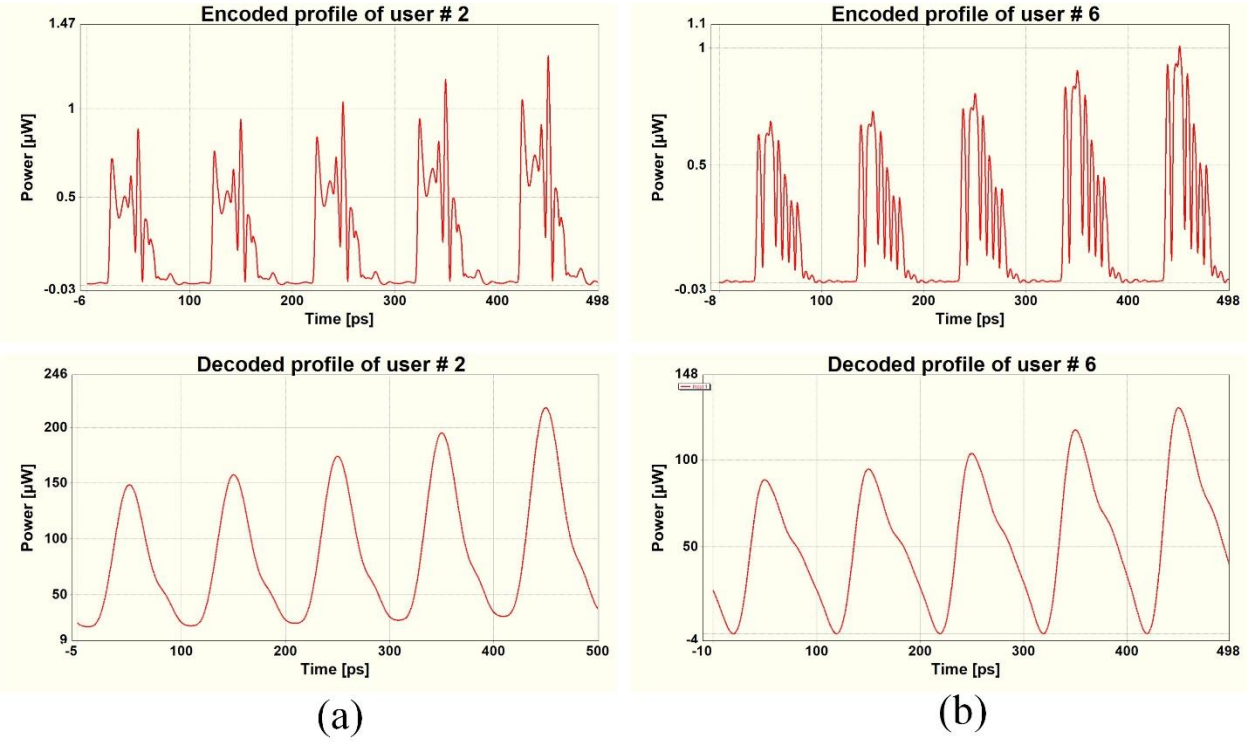

Fig. 6 Quaternary phase shift code profiles. (a) encoded profiles of users 2 and 6 (b) decoded profiles of users 2 and 6

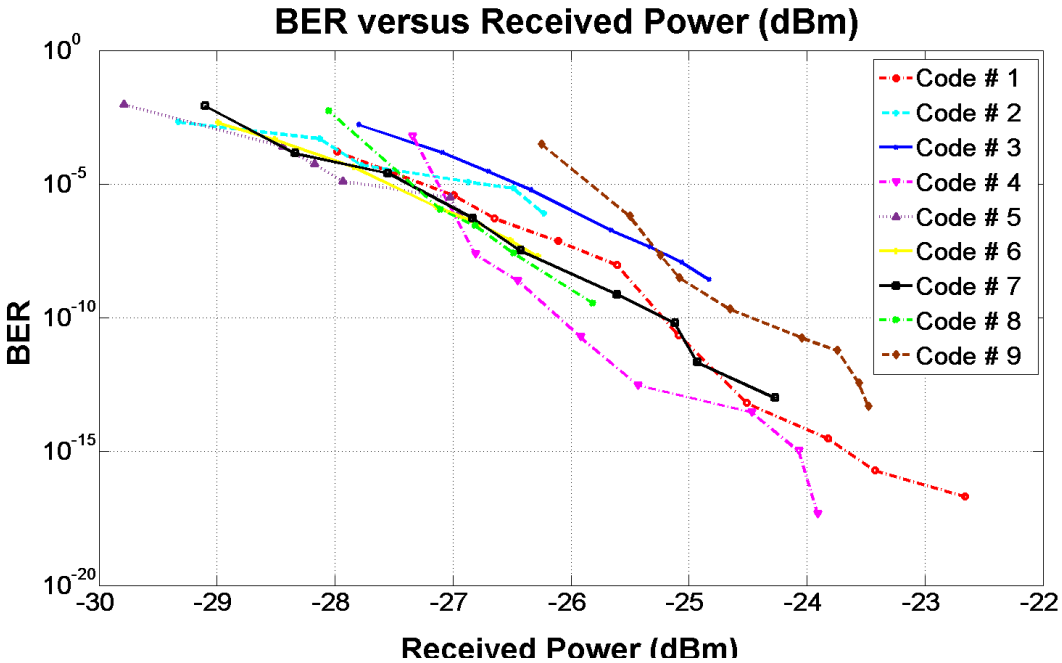

Fig. 7 BER versus the received optical power for all nine quaternary phase shift codes

5 Discussion

Based on the theoretical analysis and simulation results achieved in the previous section, the comparison of figures 4 and 6 shows that the signal encoded by the m-sequence codes has a peak with large power levels when decoded. Also, the peak width is relatively narrower than the peaks achieved from decoding the signals encoded with the quaternary phase shift codes. However, comparison of the results depicted in figures 5 and 7 shows that the BER versus the received optical power (in dBm) is improved about 20 dB from the 31-segment m-sequence codes to the 7-segment quaternary phase shift codes.

On the one hand, the decoded signal is regulated by an Optical Hard Limiter unit (OHL) to equalize all the peaks' power levels to a maximum (the highest peak power) and thus, each peak's width is much narrower after the OHL. On the other hand, the BER measurement is performed after the signal is detected in a photodiode and is band pass filtered. Therefore, the

BER figure of the quaternary phase shift codes shows around 20 dB improvement compared to the m-sequence codes. In addition, the structure, features, advantages and disadvantages of each of the code families are discussed. Based on the findings of this work, quaternary phase shift codes have obvious advantages over m-sequence codes because, i) a shorter length of the code can accommodate a larger number of channels, ii) the SSFBG device that encodes/decodes these codes is less bulky, iii) the codes are more complex because of having four levels, and iv) the cross- and auto- correlation of the encoded signals for all code sequences are better than the ones for the m-sequence.

6 Conclusion

In this study, a W-band OCDMA radio-over-fiber system is presented. The 84-GHz signal is generated by utilizing a tandem DE-MZMs. The theoretical analysis for the optical signal, after generation up until optically encoding in the SSFBG device, are presented. This system simultaneously transmits six encoded signals for six channels along with an unmodulated carrier through a 50-km length of fiber. Finally, simulation results of the photonic generation of a millimeter wave signal that is encoded and decoded by both sets of codes are presented. The theoretical analysis and the simulation results that are presented in this work can be used to design a system where a millimeter wave signal carries many channels of data to a destination. The destination can be a millimeter wave antenna retransmitting the converted electrical signal. The retransmitted millimeter wave over the air can be used to cover a micro/nano cell according to the upcoming mobile phone communication architecture.

Also, the guidelines suggested in this study defines a selection criterion to find a more effective and optimised set of optical codes for a given number of channels by simply choosing the number of segments of the SSFBG device.

In general, this study demonstrates that a system transmitting millimeter wave signals in the W-band window can carry encoded data of multiple channels to tens of kilometres farther without introducing any degradation to the signal format. This is also reconfirmed by the achieved BER versus received optical power curves for different optical code sets.

The continuation of this research will involve investigating the effect of increasing the number of channels by the introduction of the WDM technique on the encoded/ decoded profile and the BER of the received optical signal. Also, alternative quaternary phase shift codes with increased code length and the different characteristic polynomial equation, can be implemented to enhance the capabilities of the system.

References

1. T. S. Rappaport, G. R. MacCartney, M. K. Samimi, et al., "Wideband Millimeter-Wave Propagation Measurements and Channel Models for Future Wireless Communication System Design," IEEE Transactions on Communications, 63(9), pp. 3029-3056 (2015)
2. S. Rangan, T. S. Rappaport, E. Erkip, "Millimeter-Wave Cellular Wireless Networks: Potentials and Challenges," Proceedings of the IEEE, 102(3), pp. 366-385 (2014)
3. '5G Radio access: capabilities and technologies' [white page], Ericsson white paper Uen 284 23-3204 Rev C, April 2016, https://www.ericsson.com/res/docs/whitepapers/wp-5g.pdf accessed 17 November 2016
4. A. Lebedev, J. J. Vegas Olmos, X. Pang, et al. "Demonstration and Comparison Study for V- and W-Band Real-Time High-Definition Video Delivery in Diverse Fiber-Wireless Infrastructure," Fiber and Integrated Optics, 32(2), pp.93-104 (2013)
5. Y. Xu, Z. Zhang, X. Li, et al., "Demonstration of 60 Gb/s W-Band Optical mm-wave Signal Full-Duplex Transmission Over Fiber-Wireless-Fiber Network," IEEE Communications Letters, 18(12), pp. 2105-2108 (2014)
6. H. T. Huang, C. T. Lin, C. H. Ho, et al., "High spectral efficient W-band OFDM-RoF system with direct-detection by two cascaded single-drive MZMs," Optics Express, 21(14), pp. 16615-16620 (2013)
7. J. Yu, G. K. Chang, Z. Jia, et al., "Cost-Effective Optical Millimeter Technologies and Field Demonstrations for Very High Throughput Wireless-Over-Fiber Access Systems," Journal of Lightwave Technology, 28(16), pp. 2376-2397 (2010)
8. Z. Jia, J. Yu, G. Ellinas, et al., "Key Enabling Technologies for Optical–Wireless Networks: Optical Millimeter-Wave Generation, Wavelength Reuse, and Architecture," Journal of Lightwave Technology, 25(11), pp. 3452-3471 (2007)

9. X. Pang, A. Lebedev, J. J. Vegas Olmos, et al., "Multigigabit W-Band (75–110 GHz) Bidirectional Hybrid Fiber-Wireless Systems in Access Networks," Journal of Lightwave Technology, 32(23), pp. 4585-4592 (2014)
10. X. Li, J. Yu, Z. Dong, et al., "Photonics Millimeter-Wave Generation in the E-Band and Bidirectional Transmission," IEEE Photonics Journal, 5(1), pp. 7900107-7900107 (2013)
11. M. Niknamfar, M. Shadaram, "Two sub-carriers multiplexed millimeter wave generation using Mach-Zehnder modulators," Transparent Optical Networks (ICTON), 2014 16th International Conference on, Graz, Austria, 2014, pp. 1-4.
12. C. Chen, C. Zhang, K. Qiu, "OCDMA-based 60-GHz radio-over-fiber system for next generation wireless access networks," Microwave and Millimeter Wave Technology (ICMMT), 2012 International Conference on, Shenzhen, China, 2012, pp. 1-4
13. P. C. Teh, P. Petropoulos, M. Ibsen, et al., "A comparative study of the performance of seven- and 63-chip optical code-division multiple-access encoders and decoders based on superstructured fiber Bragg gratings," Journal of Lightwave Technology, 19(9), pp. 1352-1365 (2001)
14. M. K. Eghbal, M. Shadaram, "Tandem-modulator generated W-band OCDMA radio-over-fiber system," 2016 18th International Conference on Transparent Optical Networks (ICTON), Trento, 2016, pp. 1-3.
15. W. Amaya, D. Pastor, R. Baños, et al. "WDM-Coherent OCDMA over one single device based on short chip Super structured fiber Bragg gratings," Opt. Express, 19(24), pp. 24627-24637 (2011)
16. X. Wang, K. Matsushima, A. Nishiki, et al., "High reflectivity superstructured FBG for coherent optical code generation and recognition," Opt. Express, 12(22), pp. 5457-5468 (2004)
17. E. H. Dinan, B. Jabbari, "Spreading codes for direct sequence CDMA and wideband CDMA cellular networks," IEEE Communications Magazine, 36(9), pp. 48-54 (1998)
18. S. Boztas, R. Hammons, P. Y. Kumar, "4-phase sequences with near-optimum correlation properties," IEEE Transactions on Information Theory, 38(3), pp. 1101-1113 (1992)

19. Y. Niu, Y. Li, D. Jin, et al., "A survey of millimeter wave communications (mmWave) for 5G: opportunities and challenges," Wireless Networks, 21(8), pp 2657-2676 (2015)
20. L. Wei, R. Q. Hu, Y. Qian, et al., "Key elements to enable millimeter wave communications for 5G wireless systems," IEEE Wireless Communications, 21(6), pp. 136-143 (2014)
21. Z. Pi, F. Khan, "An introduction to millimeter-wave mobile broadband systems," IEEE Communications Magazine, 49(6), pp. 101-107 (2011)
22. P. C. Teh, "Application of superstructure fiber Bragg gratings for optical code division multiple access and packet switched networks," Ph.D. dissertation, Dept. Elect. and Comp. Sci., Univ. of Southampton, Southampton, UK (2003)
23. M. Bakaul, A. H. M. R. Islam, A. Nirmalathas, "Recent progresses in Gigabit wireless access using millimeter-wave RoFs," IEEE 6th International Conference on Photonics (ICP), Kuching, 2016, pp. 1-3.
24. T. Yang, M. Gao, J. Qian, "A simple scheme to generate two millimeter-wave signals for radio-over-fiber systems," 8th IEEE International Conference on Communication Software and Networks (ICCSN), Beijing, 2016, pp. 478-482.
25. A. Bekkali, K. Nishimura, "Seamless convergence of radio-over-fiber and millimeter-wave links for highly resilient access networks," IEEE Wireless Communications and Networking Conference, Doha, 2016, pp. 1-6.
26. T. Erdogan, "Fiber grating spectra," Journal of Lightwave Technology, 15(8), pp. 1277-1294 (1997)
27. J. F. Huang, Y. T. Chang, C. Hsu, "Hybrid WDM and optical CDMA implemented over waveguide-grating-based fiber-to-the-home networks," Optical Fiber Technology, 13(3), pp. 215-225 (2007)
28. M. K. Eghbal, F. Aminian, M. Shadaram, "Effect of different optical codes on a W-band WDM-over-OCDMA system," 19th International Conference on Transparent Optical Networks (ICTON), Girona, 2017, pp. 1-4.

29. M. K. Eghbal, and M. Shadaram, "Tandem dual-electrode Mach Zehnder modulators generating W-band signals for an OCDMA radio-over-fiber system," 2017 IEEE Photonics Society Summer Topical Meeting Series (SUM), San Juan, pp. 213-214 (2017)
30. M. K. Eghbal, and M. Shadaram, "W-band radio-over-fiber propagation of two optically encoded wavelength channels," Opt. Eng. 57(1), 016104 (2018)
31. S. M. Lin, J. F. Huang, C. C. Yang, "Optical CDMA network codecs with merged-M-coded wavelength-hopping and prime-coded time-spreading," Optical Fiber Technology, 13(2), Pages 117-128 (2007)
32. X. Chen, D. Huang, X. Yuan, "A grating-based 40 Gb/s OCDM coding-decoding system," Proc. SPIE 6021, Optical Transmission, Switching, and Subsystems III, 6021(2I), pp. 646-653 (2005)
33. I. Glesk, Y. K. Huang, C. S. Brès, P. R. Prucnal, "Design and demonstration of a novel optical CDMA platform for use in avionics applications," Optics Communications, 271(1), pp. 65-70 (2007)
34. B. Dai, et al., "Performance comparison of 0/pi- and +/- pi/2-phase-shifted superstructured Fiber Bragg grating en/decoder," Optics Express, 19(13), pp. 12248-12260 (2011)
35. J. S. Pereira, H. J. A. da Silva, "Error probability upper bound for perfect sequences implemented with super-structured fiber Bragg gratings," IET Signal Processing, 8(4), pp. 421-428 (2014)
36. S. A. Miraftabzadeh, P. Rad, M. Jamshidi, "Efficient distributed algorithm for scheduling workload-aware jobs on multi-clouds," 11th System of Systems Engineering Conference (SoSE), Kongsberg, 2016, pp. 1-8.
37. T. A. Pham, et al., "Performance analysis of MMW/RoF link in broadband optical-wireless access networks," 3rd National Foundation for Science and Technology Development Conference on Information and Computer Science (NICS), Danang City, 2016, pp. 153-158.
38. T. Dat, et al., "Millimeter- and terahertz-wave radio-over-fiber for 5G and beyond," IEEE Photonics Society Summer Topical Meeting Series (SUM), San Juan, 2017, pp. 165-166.
39. T. Dat, et al., "5G transport networks: the need for new technologies and standards," IEEE Communications Magazine, 54(9), pp. 18-26 (2016)

40. P. Wang, et al., “Multi-gigabit millimeter wave wireless communications for 5G: from fixed access to cellular networks,” IEEE Communications Magazine, 53(1), pp. 168-178 (2015)

First Author is a post-doctoral researcher Photonics Research Lab at the University of Texas at San Antonio. He received his Ph.D. degree in Electrical Engineering from the University of Texas at San Antonio and his master's degree photonics engineering from Chalmers University of Technology. His research focuses on capacity increase scenarios with millimeter wave radio-over-fiber communication, optical encoding techniques, and WDM optical networks for next generation mobile networks (5G). He has published more than 10 articles in conference proceedings.

Second Author is the Briscoe Distinguished Professor and the founding Director of the Center for Excellence in Engineering Education at The University of Texas at San Antonio. His main area of research is in the broadband analog and digital fiber optic and wireless systems. He has published more than 120 articles in refereed journals and conference proceedings. He is senior member of IEEE. He received his PhD in electrical engineering in 1984 from The University of Oklahoma.

